Implementation of Integrated VCSEL-Based Optical Feedback Interferometry Microfluidic Sensor System with Polymer Microoptics

Yu Zhao, Qingyue Li, Jean-Baptiste Doucet, Pierre-François Calmon, Fabien Mesnilgrente, Benjamin Reig, Clément Tronche, Thierry Camps, Julien Perchoux, Véronique Bardinal

applied sciences

MDPI

Article

Implementation of Integrated VCSEL-Based Optical Feedback Interferometry Microfluidic Sensor System with Polymer Microoptics

Yu Zhao [1,2,3], Qingyue Li [1], Jean-Baptiste Doucet [1], Pierre-François Calmon [1], Fabien Mesnilgrente [1], Benjamin Reig [1], Clément Tronche [1], Thierry Camps [1], Julien Perchoux [1] and Véronique Bardinal [1,*]

1 LAAS-CNRS, Université de Toulouse, CNRS, INP, UPS, F-31400 Toulouse, France; zhaoyuile@bjut.edu.cn (Y.Z.); qli@laas.fr (Q.L.); jbdoucet@laas.fr (J.-B.D.); pierre-francois.calmon@laas.fr (P.-F.C.); fabien.mesnilgrente@laas.fr (F.M.); breig@laas.fr (B.R.); clement.tronche@laas.fr (C.T.); camps@laas.fr (T.C.); perchoux@laas.fr (J.P.)

2 Institute of Laser Engineering, Beijing University of Technology, Beijing 100124, China

3 Beijing Engineering Research Center of Laser Technology, Beijing 100124, China

* Correspondence: bardinal@laas.fr; Tel.: +33-561-337-836

Received: 18 November 2019; Accepted: 9 December 2019; Published: 13 December 2019

check for updates

Abstract: Using the optical feedback interferometry (OFI) technique, we demonstrated a miniaturized and compact sensor system based on a dedicated optical source for flowmetry at the micro-scale. In the system, polymer microlenses were integrated directly on a VCSEL (vertical-cavity surface-emitting laser) chip and the microfluidic channel chip surface using polymer-based micro-fabrication technologies. In particular, at a post-process stage, we integrated a collimation lens on a VCSEL chip of small dimensions (200 µm × 200 µm × 150 µm). This process was enabled by the soft-printing of dry thick resist films and through direct laser writing technology. We performed flow rate measurements using this new compact system, with a conventional bulk glass lens configuration for system performance evaluation. A maximum 33 dB signal-to-noise ratio was achieved from this novel ultra-compact system. To our knowledge, this is the highest signal level achieved by existing OFI based flowmetry sensors.

Keywords: microfluidic; doppler; laser sensing; integrated microoptics; micro-nano; technology; VCSEL; laser beam shaping

1. Introduction

The development of micro-nano technologies, integrated microfluidic systems has emerged as a widely used scheme for "lab on a chip" device miniaturization. Such systems have been used in various medical and chemical applications, e.g., chemical analysis and synthesis, two-phase mixing, and particle sorting [1–3]. Many of these topics, such as flow cytometry, particle counting, and droplet generation, require the accurate measurement and control of flow rate within the microfluidic channels [4–7]. Thus, a flowmetry sensor is an essential component in the microfluidic systems.

Given its own intrinsic advantages, in particular, lowered cost, design simplicity, and high accuracy, optical feedback interferometry (OFI) has drawn great attention in metrology research [8–12]. In an OFI sensor, a part of the laser radiation is reflected or back-scattered from the distant target, and the back-propagating radiation re-enters the laser cavity where it interferes with the original laser wave. It results in a variation of the laser output power or its junction voltage [13,14]. In the case of a velocity measurement, the back-scattered wave frequency will be shifted due to the Doppler effect. Thus, the laser power variation will be a periodic function with a frequency f_D that can be expressed as:

$$f_D = \frac{2V \cdot sin\theta}{\lambda}, \tag{1}$$

where λ is the laser wavelength, V is the target velocity, θ is the incident angle formed by the laser propagation axis and perpendicular to the channel chip.

OFI based microfluidic sensors have been reported since the last decade [15]. Using this technique, Campagnolo et al. implemented a flowing velocity profile measurement system. This was done in a polydimethylsiloxane based elastomer (PDMS) microchannel with a 320 μm internal diameter, thereby achieving a clear and outstanding Doppler spectral peak in the signal spectra [16]. Miquet et al. enabled the velocity profile measurement of milk-oil two-phase flow in a Y-shaped microchannel [17]. In a previous publication, the authors had demonstrated a reasonable OFI based on a flowmetry spectral signal in a 100 × 100 μm square microchannel [18]. However, in the existing sensing systems, the optical configurations were bulk and suffered from a delicate alignment of free-space optics to couple the laser beam to the microchannel. Thus, a miniaturized OFI sensing system without the bulk optics, that can be integrated with the microchannel, is preferable. Milan Nikolić et al. [19], for the first time, facilitated the miniaturization of the OFI sensor using an optical fiber coupling inside the channel chip and achieved reasonable measurement results. However, in their work, the signal level was considerably lower than the standard bulk configuration, where a maximum 15 dB signal-to-noise ratio (SNR) was reached. Therefore, sensitive and robust integrated OFI flowing sensor systems are still required.

In this work, based on the use of the vertical-cavity surface-emitting lasers (VCSELs), we proposed the design of a micro-scale OFI flowmetry sensor system by integrating micro-optical elements directly on the top surface of the VCSEL chip and on the microchannel surface. We describe the fabrication process, discuss the technological constraints that were addressed, and present a set of results that highlight the experimental performances of our novel home-made system. The paper is constructed as follows: first, the fabrication procedure of the micro-scale component (lens on laser and microfluidic channel) is described in detail. Second, the electronic and optical characteristics are investigated to analyze the laser output performance. Finally, the flowmetry measurement is performed using this new compact system. The results are compared with the ones obtained using a traditional bulk glass lens pair to investigate the system sensitivity.

2. Device Fabrication

As shown in Figure 1, the miniaturized OFI sensor microfluidic sensing system consists of two parts. First, a VCSEL-based OFI sensor with an integrated micro-lensing system for beam collimation. Second, a microfluidic chip on which a micro focusing lens has been deposited. This geometry presents many advantages. First, it is very compact as it does not require any macro-optical elements. Second, as the laser beam is collimated, the distance between the source and the channel is not a critical parameter to obtain a sharply focused spot (size <20 μm) at the channel center.

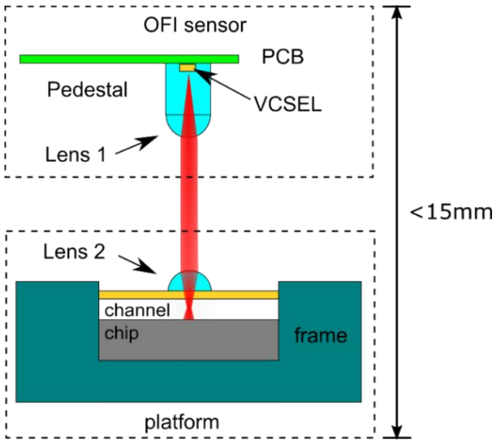

Figure 1. Schematic of the miniaturized optical feedback interferometry (OFI) flowmetry sensor system.

2.1. Fabrication of the Collimated VCSEL on PCB

As low power consumption devices with a circular output beam shape and ease of coupling to optics and fibers, VCSEL chips offer unique advantages for fabricating compact optical sensors. We chose polarization-stable VCSEL chips (referred to as ULM850-A4-PL-S46XZP Philips, CO., LTD) emitting at 850 nm. The natural full far-field beam divergence angle ($1/e^2$) was measured to be about 14°. To reduce this value, we integrated a polymer collimation microlens directly above the chip after the dicing step. It was composed of a microlens deposited on a pedestal with a high aspect ratio [20] and a typical height of at least 100 µm. The micro-scale component dimensions (pedestal diameter and height, lens radius of curvature, and height) were optimized using the ZEMAX optical software. This was done to minimize laser beam divergence (<3°) and beam size (<60 µm) at a distance of 1 mm (corresponding to the distance to the surface of the microfluidic channel).

In the literature, the direct integration of microlens on VCSELs is only reported at the wafer-scale, mainly using standard photolithography [21–26]. As these methods are not applicable to single chips, we developed an alternative method (as shown in Figure 2) to enable similar integration on single VCSELs chips of a very small size (200 µm × 200 µm × 150 µm). It was based on three micro-optical fabrication steps: soft thermal printing (alternative to standard spin-coating), direct laser writing (alternative to standard UV-photolithography), and inkjet printing.

First, the VCSEL chip was assembled on a printed circuit board (PCB) (Figure 2a). Three commercial dry thick photoresist films (DF-1050) were then transferred onto the VCSEL chip surface using soft-thermal-printing by means of nanoimprint equipment (Nanonex NX-2500). This equipment is suitable for handling brittle and small-sized samples (Figure 2a–d). This technique was previously developed by the authors to optimize the uniformity of thick resist layers on GaAs samples (a quarter of a wafer with a surface of a few cm^2) [27]. As the nominal thickness of a single DF-1050 film is only 48 µm, three films had to be successively printed on the chip to obtain a pedestal height greater than 100 µm.

Moreover, it is worth noting that due to the higher pressure applied during printing on the very small-sized VCSEL chip (compared to printing on a sample of a larger surface), the final film height measured after development was lower than the expected value (136 µm instead of 144 µm). Nevertheless, this height was found to be reproducible (standard deviation: ±5 µm). Moreover, this parameter is not critical as the lens curvature radius can be adjusted in the final step as a function of the effective pedestal height (see step (g)). Then, using direct UV laser writing (DILASE 750), high aspect-ratio cylindrical pedestals were photo-patterned in the printed films (typical diameter: 80 µm). This technique provides the same alignment precision to standard photolithography (±1 µm), leading to good pedestal centering with the VCSEL source located 136 µm below (Figure 2e). After pedestal development and curing (Figure 2f), the inkjet printing technique was used to dispense commercial SU8-based liquid microdroplets of low viscosity (PriElex, MicroChem Co., Ltd.) on the pedestal surface (Figure 2g). This technique leads to a self-centering of the polymer microlens obtained after UV-curing. The radius of the curvature of the lens was controlled precisely by the number of printed droplets, and it was previously calibrated using confocal optical microscopy. Finally, wire bonding could be performed to connect all the lensed-lasers (Figure 2h).

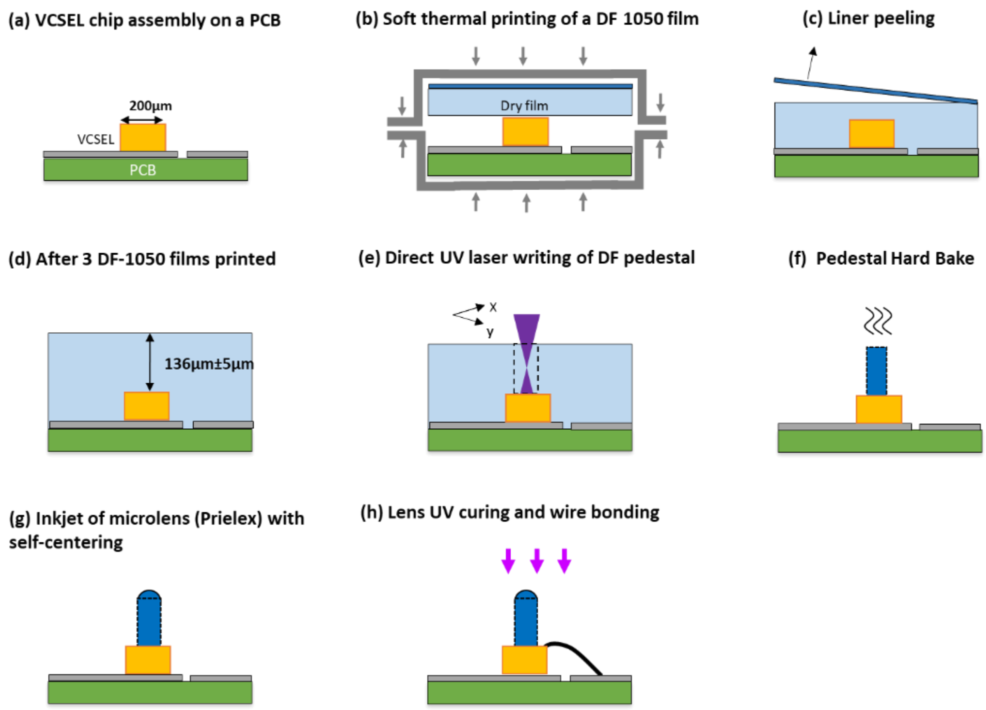

Figure 2. Process flow for microlens integration on a single vertical-cavity surface-emitting laser (VCSEL) chip already assembled on printed circuit board (PCB): (**a**) VCSEL chip assembly, (**b**) Soft-thermal printing of DF-1050 dry photoresist film, (**c**) Peeling of the liner's film, (**d**) Result after 3 soft-printing of DF-1050 films, (**e**) Direct UV laser writing on the printed films for pedestal definition, (**f**) Pedestal hard-bake, (**g**) Inkjet printing of Prielex resist on the pedestal surface, (**h**) UV curing of microlens and wire bonding.

Figure 3 shows the SEM (scanning electron microscope) images of a device after pedestal fabrication (Figure 3a) and after lens integration (Figure 3b), as well as a zoom illustrating the good surface quality of the lens (Figure 3c) and a general view of different VCSELs chips after wire bonding (Figure 3d). Such technology offers a new, efficient, cheap, and straightforward solution for single or multiple VCSEL chip(s) collimation(s) at a post-dicing stage.

To verify the collimation effect of our microlens, we measured the divergence angles of the bare VCSELs and lensed VCSELs in the same mode. The applied current in both cases was fixed at 3 mA, and the typical divergence curves obtained before and after lens integration are shown in Figure 4a. The full $1/e^2$ divergence angle of the VCSELs could be effectively decreased from 14° (in red) down to 2.9° (in blue). The maximal variation observed on the final beam divergence of the five different VCSEL chips shown in Figure 3d was 2.68 ± 0.27°, demonstrating the good reproducibility of the developed fabrication method. We also performed light-current characterizations to evaluate the VCSEL performances after lens integration. As seen in Figure 4b, only a slight modification of the L-I-V curve was observed. The threshold current of the VCSEL without lens was around 1.3 mA, while the current for the lensed-VCSEL was 1.5 mA. This phenomenon was linked to the presence of polymer material at the VCSEL surface, as microlens insertion slightly changed the reflexion coefficient of the top mirror [28]. Finally, we checked that the DOP (degree of polarization) of all VCSELs was kept higher than 75% after lens integration.

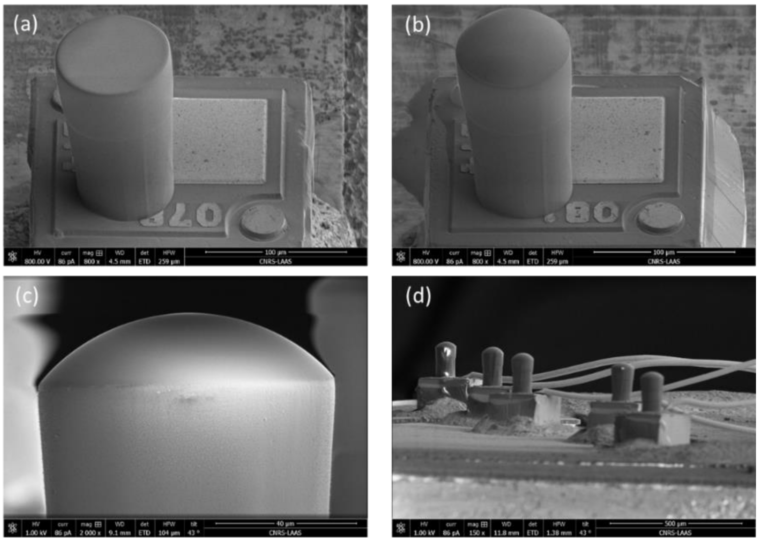

Figure 3. Scanning electron microscope images of VCSEL chip, including a micro-optical element. (**a**) after 80 µm-diameter DF-pedestal fabrication, (**b**) after lens fabrication with self-centering on the pedestal surface, (**c**) zoom on microlens profile, (**d**) general view of lensed-devices after final bonding step.

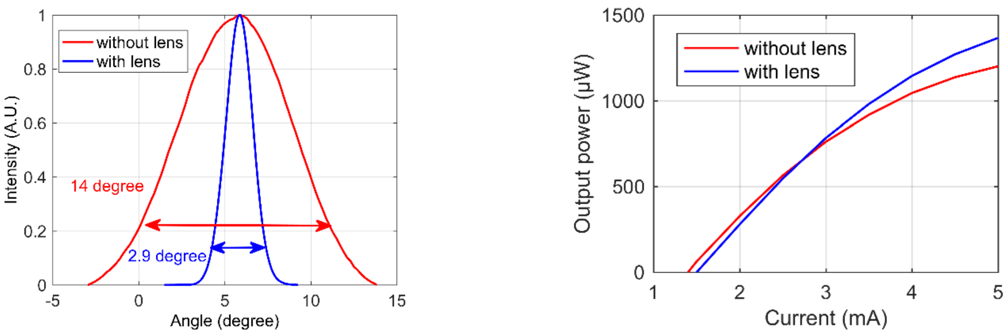

(**a**) (**b**)

Figure 4. Characterizations of VCSELs without microlens (in blue), with microlens (in red). (**a**) Full $1/e^2$ divergence angles at 3 mA current (**b**) Output current plotted as function of the current applied to the VCSEL.

2.2. Fabrication of the Microfluidic Channel with Integrated Focusing Microlens

For the reactor, a 192 µm × 192 µm square microchannel chip was fabricated by stacking four DF-1050 films using standard photolithography and lamination techniques on a glass substrate. A microlens of the same size as the VCSEL (diameter 80 µm) was printed on the top surface on the chip for laser beam focusing at the center of the channel. A general view of the microfluidic platform is shown in Figure 5a. In this case, microlens centering on the channel was achieved by means of localized surface treatment (SAM, for self-assembled monolayer) applied before the inkjet printing step. Figure 5b shows an image of the lenses fabricated on the top surface of the central part of the microfluidic channel.

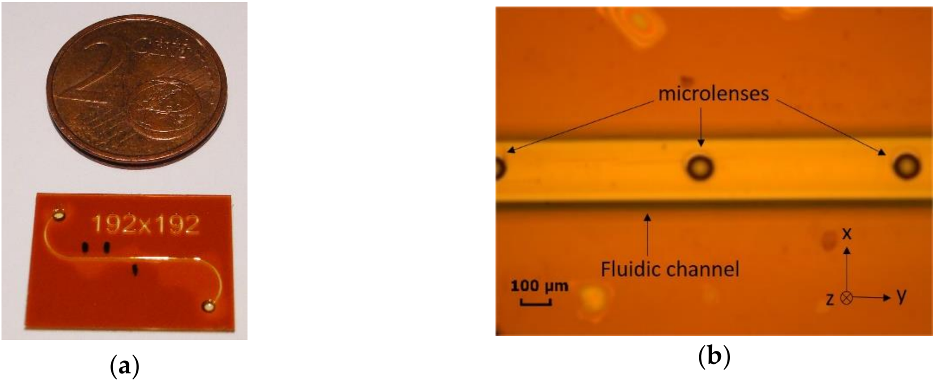

Figure 5. Photograph of the microfluidic chip: (**a**) View of the entire serpentine channel chip and size comparison with a coin of 0.7 inches in diameter (**b**) Zoom on the central part of the microchannel with focusing microlenses deposited on the surface. The lenses are positioned at the center of the channel in the X direction and spaced 500 µm apart in the Y direction.

To optimize focalization, we simulated using the ZEMAX software, the laser beam propagation along the Z-direction through the channel via the microlens scheme. We also compared this configuration to the case of a conventional C240TME-B commercial bulk lens pair. In Figure 6a,b, in the micro-scale scheme, the focused spot size in the cross-section of the channel (X-Z plane) close to the channel was distinctly smaller than the one in the bulk case (by a factor 130). Moreover, the laser incident beam focusing effect on the channel was significantly higher (Figure 6c). This improvement was expected to provide a much better spatial resolution and, as a consequence, a higher OFI signal level.

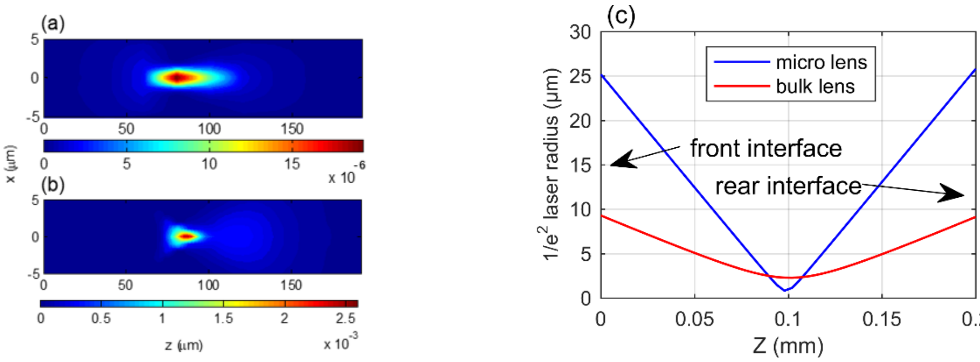

Figure 6. Modeling of laser incidence irradiation profile in the cross-section of the microchannel (X-Z plane) (ZEMAX). (**a**) Via bulk glass optical setup, (**b**) via miniaturized microlens set-up, (**c**) laser beam waist radius profile through the microchannel along the Z direction in both cases.

3. Microfluidic Flowmetry Measurements

Here, a series of flow rate measurements inside a 192 × 192 µm DF micro-channel were applied to investigate the sensing performance of two OFI systems. First, we tested a standard VCSEL chip in TO46 package mounted onto a laser mount (224 TEC TO-Can Laser Mount, Arroyo Instruments) without microlens on the laser and no lens on the channel. This basic setup served as a reference, and it is shown in Figure 7a, where the inset indicates the bulk glass lens pair. In the secondary measurements, we used the new miniaturized system proposed above as the sensor scheme. The entire setup is sketched in Figure 7b. In both cases, the incident angle between the laser axis and the normal to the channel was around 10 degrees. This value was selected because, for the integrated lens system, it is a good trade-off between the Doppler frequency shift and the minimum possible distance from the PCB to the channel chip. In this configuration, the distance from the integrated sensor to the channel top surface was around 1 mm, and the collimation beam diameter was approximately 40 µm. The focusing lens could efficiently collect this on the channel surface. Of course, because of the bulk optics, the operating distance for the basic setup is much higher (around 8 mm). In both optical configurations, the sensor position was controlled by micrometric translation stages. It was set so that the acquired signal spectrum showed the highest amplitude in the frequency domain of interest.

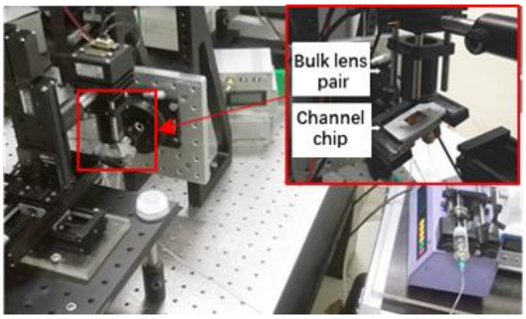

(**a**)

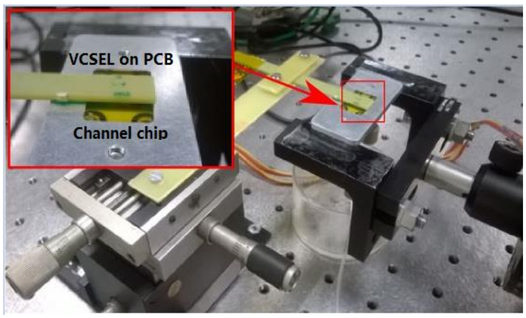

(**b**)

Figure 7. Comparative schematic of the OFI flowmetry sensor setups in microfluidic measurements. (**a**): Conventional commercial bulk lens-pair-based system. The inset presents the optical arrangement. (**b**): Integrated VCSEL-based system involving the sensor and a micromechanical stage for lateral position adjustment. The inset displays the fluidic platform and the backside of the PCB with lensed VCSEL.

The tracing object, 4.89 µm Polystyrene Spheres (PS) aqueous solution with a concentration of 0.1% w/v was pumped into the channel using a syringe pump (PHD 22/2000 Harvard Apparatus). By precisely varying the pumping flow rate, we could verify the system sensing performance robustness over a flow rate ranging from 5 to 30 µL/min. The OFI signal was acquired through the junction voltage of the VCSEL. The signal was amplified using a custom made amplifier and using a National Instrument acquisition card (NI USB 6251) at a sampling frequency of 400 kHz. Processing of the signal consisted of 30 averagings of the fast Fourier transform (FFT) of 2^{15} samples length. Thus, the total acquisition window length was 983040 (30×2^{15}). A dedicated LabVIEW program automates all the data acquisition procedures and processing.

We evaluated the signal visibility over the available laser biasing current range to find the optimal current value at which the OFI sensors could lead to the maximal signal. The OFI flowmetry measurements were repeated within applied laser operation currents ranging from 1.5 mA (threshold current value) to 3.5 mA at a 10 µL/min flow rate. The resulting OFI signal frequency spectra are depicted in Figure 8. It should be noted that when the current was set to be 1.5 mA, the OFI modulation was too weak. The OFI frequency spectral signal was overwhelmed by the system noise floor and it could hardly be observed. Moreover, all over the considerable current range, the spectrum presented a well-defined Gaussian-shaped peak. The Doppler frequency and the signal level can be calculated automatically by fitting a Gaussian function [16].

The signal level profiles as a function of the current are depicted in Figure 9. The spectral signal increases with the current, whereas when the current was set at 3 mA, the OFI signal level achieved a maximal value (around the 33 dB). This signal level was 16 dB higher compared to the bulk lenses. Moreover, even when the current is continuously increased beyond 3 mA, the OFI signal remains constant [29].

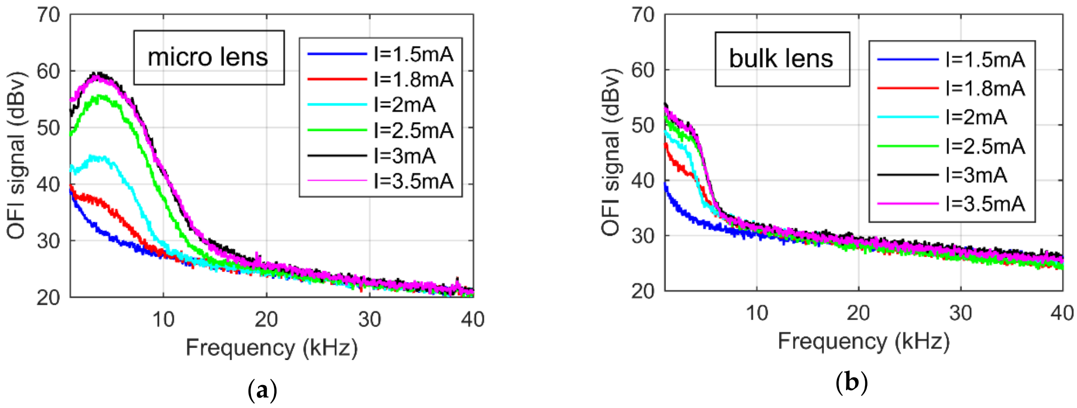

Figure 8. Frequency spectra at different currents. (**a**) The miniaturized lensed system, and (**b**) bulk glass lens system.

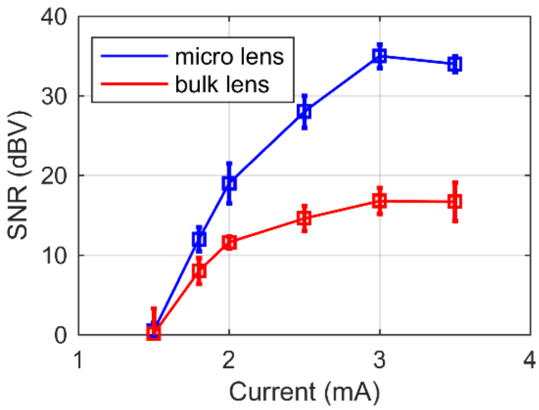

Figure 9. The signal level measured as a function of the current with error bars: miniaturized lensed system (in blue), bulk glass lens system (in red).

With the microlens, the much shorter working distance (within 2mm) can efficiently reduce the light loss during the round-trip propagation and enhance the light collection efficiency. Consequently, our system can increase the OFI signal level, especially for high currents, where there is higher initial divergence.

4. Conclusions

To summarize, a compact VCSEL laser diode-based OFI microfluidic flowmetry sensor system was fabricated using innovative additive manufacturing techniques based on commercial photoresists. To achieve maximal sensitivity, an integrated collimating microlens on the VCSEL chips, as well as a focusing lens on the top surface of the channel chip, were designed and fabricated using dry thick resist film soft-transfer, direct laser writing, and inkjet printing. We obtained a significant reduction of the laser beam divergence (division by 5), as well as an efficient beam focusing at the center of the channel (beam size <20 µm).

To validate the sensing capability of this new system, we performed flow rate measurements in a microchannel with polystyrene particles as the tracing targets. The proposed miniaturized lensed system exhibited an outstanding signal level (higher by 16 dB compared to the standard bulk glass doublet lenses configuration tested under similar experimental conditions). These results demonstrated that our sensor could satisfy the flowing sensing requirements even in extremely tiny channels. To the best of our knowledge, this is the highest signal level in the existing relevant literature. We believe this miniaturized system can be a potential tool in the design of future lab-on-a-chip devices requiring precise and sensitive flowing velocity monitoring.

Author Contributions: Conceptualization, T.C., J.P., and V.B.; Formal analysis, Y.Z., and Q.L.; Funding acquisition, J.P. and V.B.; Investigation, Y.Z., Q.L., J.-B.D., P.-F.C., F.M., B.R., C.T., and T.C.; Project administration, J.P. and V.B.; Resources, J.-B.D., P.-F.C., F.M., B.R., and C.T.; Software, Y.Z., and Q.L.; Supervision, T.C., J.P., and V.B.; Validation, Y.Z., and Q.L.; Visualization, Y.Z., Q.L. and B.R.; Writing—original draft, Y.Z.; Writing—review & editing, J.P. and V.B.

Funding: This research was funded by the Agence Nationale de la Recherche (ANR) (grant number: ANR-15-CE19-0012 DOCT-VCSEL) and the China Scholarship Council (CSC).

Acknowledgments: The authors acknowledge RENATECH (French Network of Major Technology Centers) within LAAS-CNRS, as well as Véronique Conédéra and Rémi Courson for their contribution to the DF microfluidic channel fabrication processing, and Samuel Charlot for the assembling and bonding steps. The authors also sincerely appreciate Francis Jayat for his help in the electronic designing work.

Conflicts of Interest: The authors declare no conflict of interest.

References

1. Gravesen, P.; Branebjerg, J.; Jensen, O.S. Microfluidics-a review. *J. Mioromech. Microeng* **1993**, *3*, 16–82. [CrossRef]
2. Weigl, B.H.; Bardell, R.L.; Cabrera, C.R. Lab-on-a-chip for drug development. *Adv. Drug Deliv. Rev.* **2003**, *55*, 349–377. [CrossRef]
3. Nilsson, J.; Evander, M.; Hammarström, B.; Laurell, T. Review of cell and particle trapping in microfluidic systems. *Anal. Chim. Acta.* **2009**, *649*, 141–157. [CrossRef] [PubMed]
4. Kawaguchi, T.; Akasaka, Y.; Maeda, M. Size measurements of droplets and bubbles by advanced interferometric laser imaging technique. *Meas. Sci. Technol.* **2002**, *13*, 308–316. [CrossRef]
5. Sarrazin, F.; Loubière, K.; Prat, L.; Gourdon, C.; Bonometti, T.; Magnaudet, J. Experimental and numerical study of droplets hydrodynamics in MicroChannel. *AIChE J.* **2006**, *52*, 4061–4070. [CrossRef]
6. Vennemann, P.; Lindken, R.; Westerweel, J. In vivo whole-field blood velocity measurement techniques. *Exp. Fluids.* **2007**, *42*, 495–511. [CrossRef]
7. Draijer, M.; Hondebrink, E.; Leeuwen, T.; Steenbergen, W. Review of laser speckle contrast techniques for visualizing tissue perfusion. *Lasers Med. Sci.* **2009**, *24*, 639–651. [CrossRef]
8. Zhao, Y.; Zhou, J.; Wang, C.; Chen, Y.; Lu, L. Temperature measurement of the Laser Cavity Based on Multi-longitudinal Mode Laser Self-Mixing Effect. *IEEE Sens. J.* **2019**, *19*, 4386–4392. [CrossRef]
9. Usman, M.; Zabit, U.; Bernal, O.D.; Raja, G.; Bosch, T. Detection of Multimodal Fringes for Self-Mixing-Based Vibration Measurement. *IEEE Trans. Instrum. Meas.* **2019**, *69*, 1–10. [CrossRef]
10. Wu, J.F.; Shu, F.F. Quadrature detection for self-mixing interferometry. *Opt. Lett.* **2018**, *43*, 2154–2156. [CrossRef]
11. Xu, J.; Huang, L.; Yin, S.; Gao, B.; Chen, P. All-fiber self-mixing interferometer for displacement measurement based on the quadrature demodulation technique. *Opt. Rev.* **2018**, *25*, 40–45. [CrossRef]
12. Keeley, J.; Dean, P.; Valavanis, A.; Bertling, K.; Lim, Y.L.; Alhathlool, R.; Taimre, T.; Li, L.H.; Indjin, D.; Rakić, A.D.; et al. Three-dimensional terahertz imaging using swept-frequency feedback interferometry with a quantum cascade laser. *Opt. Lett.* **2015**, *40*, 994–997. [CrossRef] [PubMed]
13. Lang, R.; Kobayashi, K. External optical feedback effects on semiconductor injection laser properties. *IEEE J. Quantum Electron.* **1980**, *16*, 347–355. [CrossRef]
14. Mitsuhashi, Y.; Shimada, J.; Mitsutsuka, S. Voltage change across the self-coupled semiconductor laser. *IEEE J. Quantum Electron.* **1981**, *17*, 1216–1225. [CrossRef]
15. Perchoux, J.; Quotb, A.; Atashkhooei, R.; Azcona, F.; Ramírez-Miquet, E.E.; Bernal, O.; Jha, A.; Luna-Arriaga, A.; Yanez, C.; Caum, J.; et al. Current Developments on Optical Feedback Interferometry as an All-Optical Sensor for Biomedical Applications. *Sensors* **2016**, *16*, 694. [CrossRef]
16. Campagnolo, L.; Nikolic, M.; Perchoux, J.; Lim, Y.L.; Bertling, K.; Loubie're, K.; Prat, L.; Rakic, A.D.; Bosch, T. Flow profile measurement in microchannel using the optical feedback interferometry sensing *technique*. *Microfluid. Nanofluid.* **2013**, *14*, 113–119. [CrossRef]
17. Ramrez-Miquet, E.E.; Perchoux, J.; Loubière, K.; Tronche, C.; Prat, L.; Sotolongo-Costa, O. Optical feedback interferometry for velocity measurement of parallel liquid-liquid flows in a microchannel. *Sensors* **2016**, *16*, 1233. [CrossRef]

18. Zhao, Y.; Perchoux, J.; Campagnolo, L.; Camps, T.; Atashkhooei, R.; Bardinal, V. Optical feedback interferometry for microscale-flow sensing study: Numerical simulation and experimental validation. *Opt. Express* **2016**, *24*, 23849–23861. [CrossRef]
19. Nikolic, M.; Hicks, E.; Lim, Y.L.; Bertling, K.; Rakic, A.D. Self-mixing laser Doppler flow sensor: An optofluidic implementation. *Appl. Opt.* **2013**, *52*, 8128–8133. [CrossRef]
20. Levallois, C.; Bardinal, V.; Vergnenègre, C.; Leïchlé, T.; Camps, T.; Daran, E.; Doucet, J.B. VCSEL Collimation Using Self-Aligned Integrated Polymer Microlenses. In Proceedings of the SPIE, Strasbourg, France, 14 May 2008; p. 6992.
21. Jacot-Descombes, L.; Gullo, M.R.; Cadarso, V.J.; Brugger, J. Fabrication of epoxy spherical microstructures by controlled drop-on-demand inkjet printing. *J. Micromech. Microeng.* **2012**, *22*, 074012. [CrossRef]
22. Chen, F.; Lu, J.; Huang, W. Using Ink-Jet Printing and Coffee ring effect to fabricate refractive microlens arrays. *IEEE Photonics Technol. Lett.* **2019**, *21*, 648–650. [CrossRef]
23. Kim, J.Y.; Brauer, N.B.; Fakhfouri, V.; Boiko, D.L.; Charbon, E.; Grutzner, G.; Brugger, J. Hybrid polymer microlens arrays with high numerical apertures fabricated using simple ink-jet printing technique. *Opt. Mater. Express* **2011**, *1*, 259–269. [CrossRef]
24. Tien, C.H.; Hung, C.H.; Yu, T.H. Microlens arrays by direct-writing inkjet print for LCD backlighting applications. *IEEE OSA J. Disp. Technol.* **2009**, *5*, 147–151. [CrossRef]
25. Bardinal, V.; Reig, B.; Camps, T.; Levallois, C.; Daran, E.; Vergnenègre, C.; Leïchlé, T.; Almuneau, G.; Doucet, J.B. Spotted Custom Lenses to Tailor the Divergence of Vertical-Cavity Surface-Emitting Lasers. *IEEE Photonics Technol. Lett.* **2010**, *22*, 1592–1594. [CrossRef]
26. Chen, W.C.; Wu, T.J.; Wu, W.J.; Su, G.D. Fabrication of inkjet-printed SU-8 photoresist microlenses using hydrophilic confinement. *J. Micromech. Microeng.* **2013**, *23*, 065008. [CrossRef]
27. Abada, S.; Salvi, L.; Courson, R.; Daran, E.; Reig, B.; Doucet, J.B.; Camps, T.; Bardinal, V. Comparative study of soft thermal printing and lamination of dry thick photoresist films for the uniform fabrication of polymer MOEMS on small-sized samples. *J. Micromech. Microeng.* **2017**, *27*, 055018. [CrossRef]
28. Ansbæk, T.; Nielsen, C.H.; Larsen, N.B.; Dohn, S.; Boisen, A.; Chung, I.S.; Larsson, D.; Yvind, K. Polymer-Coated Vertical-Cavity Surface-Emitting Laser Diode Vapor Sensor. In Proceedings of the SPIE OPTO, San Francisco, CA, USA, 23 January 2010; Volume 7615.
29. Roumy, J.; Perchoux, J.; Lim, Y.L.; Taimre, T.; Rakić, A.D.; Bosch, T. Effect of injection current and temperature on signal strength in a laser diode optical feedback interferometer. *Appl. Opt.* **2015**, *54*, 312–318. [CrossRef]